AGU PUBLICATIONS

JGR

Journal of Geophysical Research: Space Physics

RESEARCH ARTICLE

10.1002/2014JA020038

Generation and detection of super small striations by *F* region HF heating

A. Najmi[1], G. Milikh[1], J. Secan[2], K. Chiang[3], M. Psiaki[3], P. Bernhardt[4], S. Briczinski[4], C. Siefring[4], C.L. Chang[5], and K. Papadopoulos[1,5]

[1]Department of Physics and Department of Astronomy, University of Maryland, College Park, Maryland, USA, [2]NorthWest Research Associates Inc., Redmond, Washington, USA, [3]Department of Electrical Engineering, Cornell University, Ithaca, New York, USA, [4]Division of Plasma Physics, Naval Research Laboratory, Washington, District of Columbia, USA, [5]Technology Solutions, BAE Systems, Arlington, Virginia, USA

Key Points:

- Two independent diagnostic techniques were used to study SEE and SSS
- STEC indicates density perturbation grows rapidly when BUM appears in SEE
- Hysteresis is detected in the BUM, DM, and STEC potentially via two methods

Correspondence to:
A. Najmi,
anajmi1@umd.edu

Citation:
Najmi, A., G. Milikh, J. Secan, K. Chiang, M. Psiaki, P. Bernhardt, S. Briczinski, C. Siefring, C. L. Chang, and K. Papadopoulos (2014), Generation and detection of super small striations by *F* region HF heating, *J. Geophys. Res. Space Physics*, *119*, 6000–6010, doi:10.1002/2014JA020038.

Received 3 APR 2014
Accepted 12 MAY 2014
Accepted article online 31 MAY 2014
Published online 31 JUL 2014

Abstract Recent theoretical models and preliminary observations indicate that super small striations (SSS) in the plasma density with scale size of 10 cm can be excited by *F* region HF heating at frequencies close to multiples of the electron gyrofrequency. We present here new experimental results using the High Frequency Active Auroral Research Program ionospheric heater at a frequency close to the fourth electron gyroharmonic with simultaneous GPS, Stimulated Electromagnetic Emission, ionosonde, and occasional Incoherent Radar Scattering diagnostics. Differential phase measurements of GPS signals through the heated region indicated the presence of SSS with extremely high amplitude ($\delta n/n = 0.2$–0.3) at scale size comparable to the electron gyroradius. The highest amplitude of GPS scintillations coincide with the highest level of the Broad Upshifted Maximum (BUM) and occurred when the HF frequency is slightly above the fourth harmonic of the electron cyclotron frequency. Frequency sweeps indicate that the scintillation amplitude exhibits hysteresis similar to that observed for the BUM amplitude when the HF frequency is cycled about the fourth harmonic of the cyclotron frequency. The results favor a four wave parametric process as the physical mechanism of the SSS. Additional experiments allowed the determination of the excitation and decay rates of the SSS.

1. Introduction

Generation of artificial Field-Aligned Striations (FAS) of the ionospheric plasma due to *F* region *O*-mode HF heating was first discovered in experiments conducted by the Platteville HF heater [*Thome and Blood*, 1974; *Fialer*, 1974] and subsequently confirmed in numerous experiments [*Hansen et al*., 1992; *Kelley et al*., 1995; *Bakhmet'eva et al*., 1997; *Dhillon and Robinson*, 2005]. These studies demonstrated that FAS could be used as a scattering cloud for ground-to-ground VHF communications. A key parameter required to design such communications systems is the total radar scattering cross section (SCS) per unit volume [*Carpenter*, 1974]. One of the factors that determines the SCS is the wave number spectrum of artificial fluctuations of the electron density. According to *Rao and Thome* [1974], at Platteville, the value of SCS was measured to decrease by 5 orders of magnitude when the radar frequency is swept from 20 MHz to 1 GHz. This implies that the scattering of a probe signal in the GHz frequency range is expected to be negligible, which further indicates that the spectrum of density fluctuations quickly decays for wavelengths smaller than ~30 cm. However, following a suggestion of *Gurevich and Zybin* [2006], *Milikh et al.* [2008] recently observed strong perturbations of GPS signals by FAS generated by the High Frequency Active Auroral Research Program (HAARP) heater operating at ~92 dBW Effective Radiated Power. These perturbations are indicative of excitation of super small striations (SSS) on the order of 10 cm. The observations of *Milikh et al.* [2008] were performed using *O*-mode HF *F* region heating with a frequency ω that satisfied the so-called double resonance condition, namely ω resonated at the upper hybrid height with a multiple of the electron cyclotron frequency ($\omega_{\mathrm{UH}} \approx n\,\Omega_e$). Ground measurements of the differential phase of GPS signals traversing the heated region indicated high level of SSS. However, the nonlinear physics that allows generation of such SSS and its relationship to Artificial Ionospheric Turbulence was unclear. The present set of experiments coordinate GPS and Stimulated Electromagnetic Emission (SEE) observations, and include complementary diagnostics by HAARP's Digisonde and Modular UHF Ionospheric Radar (MUIR), in an effort to study the properties of SSS generated by the HAARP heater.

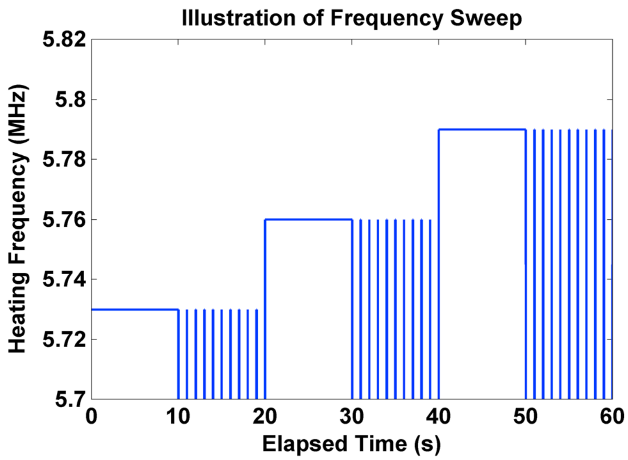

Figure 1. Illustration of frequency sweep HAARP HF heating contours (3 and 6 dB) and PRN 07 satellite tracking. Heater alternates 10 s, square pulses with a train of 20 ms, square pulses with interarrival time of 1 s. After a cycle, the heating frequency is stepped up or down by 30 kHz.

2. Description of Experiments

We report below observations from six daytime experiments, conducted during the March 2013 HAARP campaign. In the experiments, the HAARP heater operated at its maximum 3.6 MW power, *O* mode, and the HF beam was directed toward the PRN 07 satellite at 15° off zenith and 180° azimuth. PRN 07 is a GPS satellite on a geocentric orbit with inclination 55.1° to the equator, having perigee 20,143 km and apogee 20,222 km. During the experiments, PRN 07 overflew the HAARP site daily and the signals at both the L1 ($f_1 = 1.575$ GHz) and L2 ($f_2 = 1.227$ GHz) were measured on the ground after traversing the HF heated region (Figure 2) with one Hz sampling rate. The measured differential carrier phase was used to estimate the relative Slant Total Electron Content and the value of $\delta n/n$ at 20–30 cm scale length that corresponds to the Bragg condition at the GPS frequency range. Stimulated Electromagnetic Emission (SEE) signals were measured simultaneously using an HF detector operated by the Naval Research Laboratory 15 km away from the HAARP site. Data acquisition techniques have been described previously by *Bernhardt et al.* [2009, 2011]. The SEE signals are driven by the nonlinear interaction of the injected HF wave with the ionospheric plasma that results in broadband emissions at frequencies different from the injected HF frequencies [*Thide et al.*, 1982]. They are usually upshifted or downshifted from the heater frequency within a range of 100 kHz. All the experiments were also diagnosed by the HAARP ionosonde and when the geometry permitted by the site Incoherent Scatter Radar (MUIR).

The experiments were conducted using square pulse HF heating with 10 s pulse width and 10 s interpulse period. In order to determine the turn-on and decay times of the excited striations, a train of short, square, 20 ms pulses, at the heating frequency of the preceding 10 s pulse, and with an interpulse time 1 s was applied between the long, 10 s pulses as shown schematically in Figure 1.

The HF frequency selection was constrained by two requirements: First, to maintain the HF frequency f_0 below the F_2 layer critical frequency ($f_0 < f_oF_2$), and second, to operate in the vicinity of the double resonance condition ($f_{UH} \approx \mathbf{nf_{ec}}$). During the experiments, the f_oF_2 was approximately 6–7 MHz. As a result, the double resonance could be satisfied in the vicinity of the fourth electron gyroharmonic close to 5.8 MHz. The heater operation was as follows: Starting at 300–500 kHz below the fourth gyroharmonic, the heating frequency was stepped up by 30 kHz every 20 s until it reached 5.9–6.0 MHz. On 11 March 2013, the heating was terminated after reaching ~6.0 MHz. On subsequent days, the frequency was cycled back after reaching 6 MHz in 30 kHz steps every 20 s, thereby crossing the expected gyroharmonic from above and below.

The critical diagnostic instrument is a GPS receiver located at HAARP that detects the changes in the phase of the GPS signals sent from satellite PRN 07 crossing the heated region and received at HAARP. Other important diagnostic instruments were a broadband HF receiver operated by the Naval Research Laboratory that measured SEE signals, the site ionosonde that measured the plasma density profile above the site and the MUIR radar that measured plasma waves excited by the heater.

Table 1 lists the key parameters of the experiments, including experiment times and ionospheric conditions. During all the experiments, the on-site diagnostics indicated a smooth *F* region layer, weak to moderate *D* and *E* region absorption, and the absence of electrojet current. Moreover, the HAARP magnetometer showed small variations of the geomagnetic fields (<20 nT), indicating a quiet ionosphere.

Table 1. Key Experimental Information, Including the Experimental Time, the Heating Regime, the HF Frequency (f_0), and the Critical Frequency (f_oF_2)[a]

	HF Heating Time (UT)	HF Heating Pattern	HF Heating Frequency	f_oF_2 (MHz)	Notes
#1	01:05:00–01:14:30 3/11/2013	10 s on/10 s off	From 5.3 MHz stepping up to 5.9 MHz by 30 kHz every 20 s	5.7–6.8	
#2	01:00:00–01:09:30 3/12/2013	10 s on/10 s off	From 5.5 MHz stepping up to 5.9 MHz and then from 6.8 to 7.0 MHz by 30 kHz every 20 s	6.7–7.4	
#3	00:55:00–01:04:10 3/13/2013	10 s on/10 s off	From 5.5 MHz stepping up to 5.9 MHz by 30 kHz every 20 s, then stepping down with the same rate	6.1–7.7	Overshoot in slant TEC detected
#4	00:50:00–00:59:40 3/14/2013	10 s on/ 10 s off	Same as in experiment #3 except stepping up from 5.5 to 6.0 MHz	7.3–7.6	Overshoot in slant TEC detected
#5	00:50:00–00:59:10 3/15/2013	10 s on/10 s off	Same as in experiment #3 except stepping up from 5.6 to 6.0 MHz	6.3–7.4	Overshoot in slant TEC detected
#6	00:45:00–00:54:00 3/16/2013	10 s on/10 s off	Same as in experiment #5	6.4–6.6	

[a]TEC, total electron content.

3. Experimental Observations

Figure 2 presents an overview of the GPS experiment and the HAARP heated regions. The figure shows the tracking of satellite PRN 07 relative to the HAARP heated region, with the red and blue ovals outlining the 3 and 6 dB contours of the heated region at altitudes of 180 and 240 km on 13 March 2013 with HAARP indicated by a star. The colored lines are the projection of points where a microwave beam from the satellite directed toward the HAARP receiver, crosses a surface at the given altitude. PRN 07 was chosen for this experiment because it crosses almost directly over the center of the heated region. It takes ~10 min for the GPS signal to fully cross the heated region, and this sets the time scale of our GPS experiments.

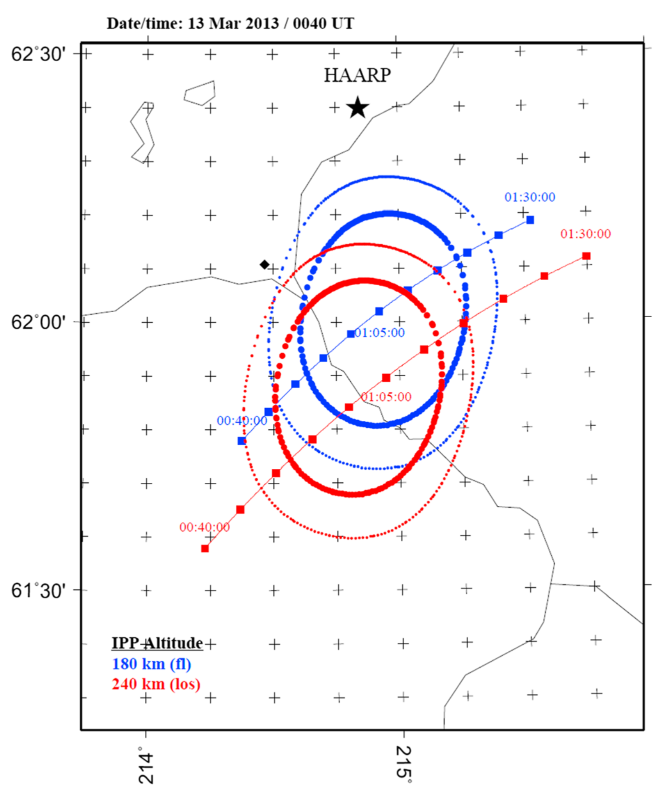

Figure 2. Heater contours and satellite tracking on 13 March 2013. HAARP HF heating contours of 3 and 6 dB at altitudes of 180 and 240 km are shown in the red and blue ovals. Crossing positions of a microwave beam from PRN 07 directed toward the HAARP receiver, at altitudes of 180 and 240 km, are indicated on the red and blue lines.

The processing of the received GPS signals was described in detail in *Milikh et al.* [2008]. It uses the observed phase ($\boldsymbol{\phi_1}$ and $\boldsymbol{\phi_2}$) of both the L1 ($f_1 = 1.575$ GHz) and L2($f_2 = 1.227$ GHz) GPS frequencies and estimates the differential carrier phase $\boldsymbol{\Delta\phi_{12}}$. The latter then was converted to relative Slant Total Electron Content (STEC) using

$$\Delta(\mathrm{STEC}) = \frac{0.75 f_1 \Delta\varphi_{12}}{f_1^2/f_2^2 - 1} \quad (1)$$

The STEC is measured in TEC units (1 TECU = 10^{16} el/m^2), the frequencies are in GHz, and the differential carrier phase is in radians. Further analysis and description of GPS phase differences caused by ionospheric scintillation is also described by *Pelgrum et al.* [2011].

Figures 3a and 3b show the absolute STEC versus the observational time measured during experiments #3 and 4, with the beginning and end of the HF

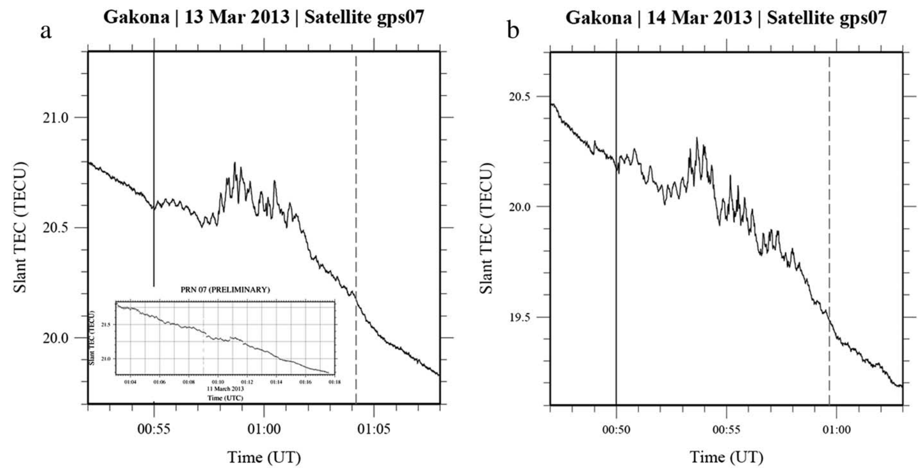

Figure 3. STEC observations made on (a) 13 March 2013 and (b) 14 March 2013. Unperturbed STEC from 11 March 2013 is included in Figure 3a for reference. The beginning and end of HF heating is indicated with solid and dashed lines, respectively.

heating shown by the two vertical lines. Notice that the STEC of the probe GPS signals changes abruptly in about 35 s following turn-on of the HF heating, and then oscillates with the 20 s heating period. As mentioned above, within minutes, PRN 07 moves from the center of the heated region, where the HF heating effect is strongest, to its periphery, producing an approximately linear decay of STEC. For comparison, the STEC obtained in the absence of HF heating was inserted in Figure 3a.

Figure 4 shows dynamic SEE spectra observed during experiment #4. The *x* axis shows the varying frequency in a bandwidth of 200 kHz centered about 5.82 MHz, while the *y* axis shows the elapsed time from 00:52:03 UT. The intensity of the observed signal is color coded. The 10 s long pulses are characterized by the pump wave: a bright, narrow line of constant frequency. The 10 s and +30 kHz separate successive long pulses. Between these long pulses, the short 20 ms pulses mentioned above are also shown (Figure 3). During the first long pulse (lower left), the SEE shows two spectral lines downshifted from the pump, known as the first and second downshifted maximum (DM). The next long pulse is dominated by the pump wave with faint evidence of a transient DM, indicative of the well-known DM suppression near the gyrofrequency [*Gurevich*, 2007]. The third long pulse shows a broad region of lower amplitude, but higher frequency than the pump. This is the Broad Upshifted Maximum (BUM), indicating that we have exceeded a multiple of the gyroresonance. The relative amplitude and frequency shift of the BUM relative to the pump wave vary with the pump frequency.

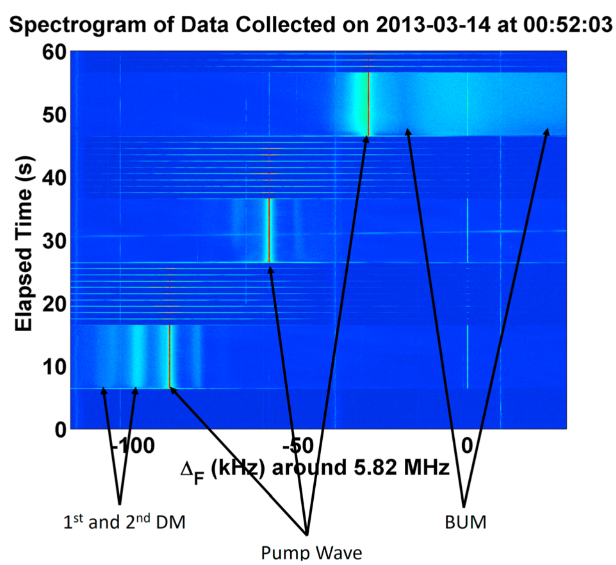

Figure 4. SEE Spectrogram from 14 March 2013. Frequency axis is centered on 5.82 MHz, and indicated pump waves are from bottom to top: 5.73, 5.76 and 5.79 MHz. For the pump at 5.73 MHz (lower left), the first and second DM are present and shifted by ~ −10 kHz and ~ −20 kHz, respectively, from the pump frequency. For the pump at 5.79 MHz (upper right), BUM is evident in the range of +10 to +50 kHz from pump frequency. The pump at 5.76 MHz (center) appears to be very close to a gyroresonance as DM is suppressed and BUM is not yet visible.

Figure 5 reveals one of the most important results of the experiments. It shows the correlation of STEC amplitude fluctuations with the power spectral density (PSD) of the SEE spectra for

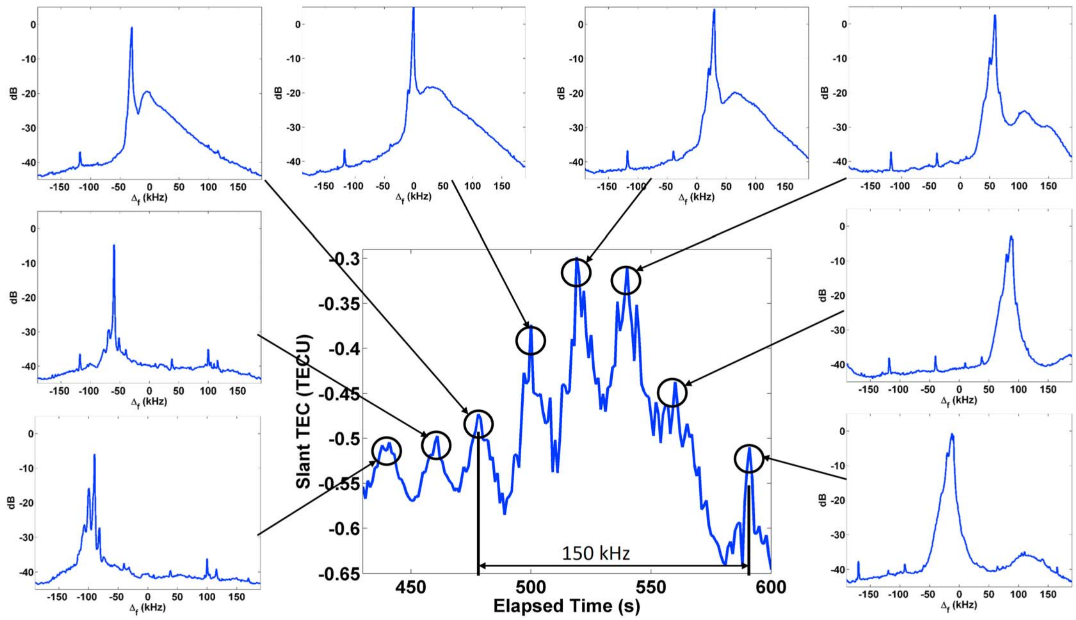

Figure 5. STEC observations near the first hump or "overshoot" made on 14 March 2013 with selected PSDs. First BUM indicated. PSDs progress in time clockwise starting from the lower left, and UT are indicated. STEC hump covers an HF heating frequency range of ~150 kHz.

experiment #4. During the first 3 min of the HF heating, the peaks of the STEC are associated with the presence of DM on the SEE spectrum. The BUM first appears at 00:53:16 UT, approximately 3 min from the beginning of heating and remains for ~2 min which corresponds to a shift in the heating frequency of ~150 kHz. During that time, the STEC shows large-amplitude oscillations, by up to 4 dB larger than during the first 3 min. The BUM is associated with a rising amplitude of the STEC and is coincident with the first of two overshoots (or humps). The first "hump" lasts for ~1.5 min and the second starts at ~00:55:06 UT and lasts for ~1 min. In these humps, the value of the STEC changes by up to 0.3 TECU and the SEE spectrum shows that a BUM is being excited.

Figures 6a and 6b show ionograms made at 2 and 4 min during the HF heating on 14 March 2013, along with the PSD of the nearest long pulse heating cycle. We found that in the first case, the SEE spectrum shows a DM, while in the latter case, the BUM has developed. At the same time, the latter ionogram indicates a spread *F* layer. In addition, during these times, the STEC transitions from small (~0.05–0.07 TECU) near 00:52:00 UT to larger (~0.15–0.20 TECU) near 00:54:00 UT. Due to angular limitations of HAARP's MUIR instrument, it is difficult to detect this turbulence directly. In spite of this difficulty, a single successful MUIR measurement was made on 14 March 2013 during the period 00:52:10–52:20 during which time $f_0 < 4\ f_{ce}$. It shows strong reflection in 200–203 km range (illustrated in Figure 7) that lasted for over 2 s followed by a faint signal that lasted for 8 s. During that time, the SEE spectrum reveals the DM, 2DM, 3DM, and upshifted maximum features although the BUM was absent. GPS measurements indicated small STEC (~0.05−0.07 TECU) oscillations during this time. We will discuss these findings further in subsequent sections.

3.1. Hysteresis Effect

In four of the experiments (#3–#6), the heating frequency was swept from $f_0 = 5.5$ MHz that corresponds to 4 f_{ce} to 300 kHz up to $f_0 = 6$ MHz, ~100–150 kHz above the BUM pumping frequency, and then cycled downward to 5.5 MHz. Detailed comparison revealed a difference between the PSDs recorded during up and down frequency sweeps. This is shown in Figures 8a–8c for experiments #3 and #4. Figure 8a shows PSDs in the frequency range around the BUM and reveals that PSDs during the upward sweep have higher amplitude than those obtained during the downward sweep. Similarly, the PSDs in the frequency range around the DM (Figure 8b) shows the hysteresis behavior. However, contrary to Figure 8a, the up sweep PSDs have lower amplitude than those during the down sweep. Hysteresis of the BUM is consistent with the observations of *Carozzi et al.* [2002]. Hysteresis of the DM is consistent in magnitude, but we observe a switch in the relative amplitude of the up and

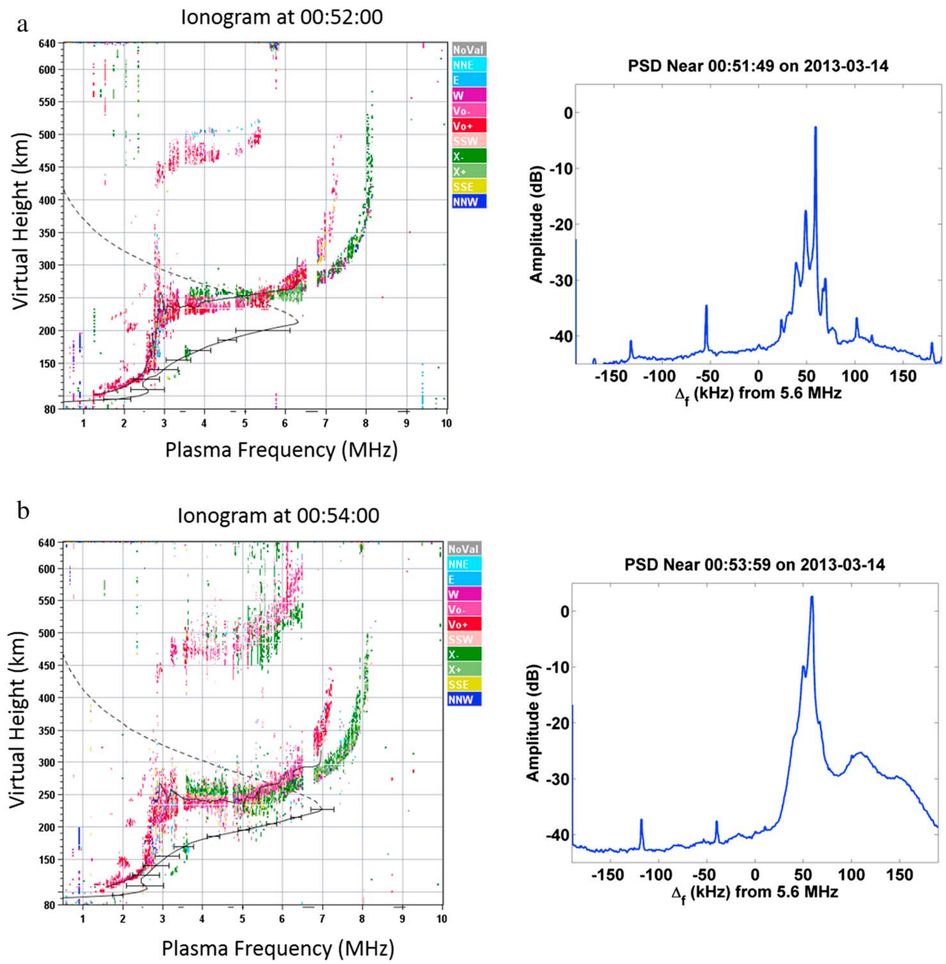

Figure 6. Ionograms taken at HAARP 14 March 2013 at (a) 00:52:00 and (b) 00:54:00 UT by the Digisonde, with associated SEE PSD. Note the broadening of ionogram in the presence of BUM. First ionogram indicates a compact *F* layer and is correlated with a DM in the SEE spectrum, while the second ionogram indicates a spread *F* layer and is correlated with a BUM in the SEE spectrum.

down sweeps. We also present in Figure 8c that hysteresis obtained from the STEC data normalized by their peak. Being strongly affected by BUM, the STEC mimics the behavior of the BUM hysteresis shown in Figure 8a.

3.2. Excitation and Relaxation Times

During various experiments, we operated with the heater off during selected periods. This gave us an opportunity to investigate the excitation and relaxation times of both the BUM and the DM. Our results are summarized in Table 2. For the DM excitation, we sliced the spectrograms of the SEE data along constant time and inspected the resulting frequency spectrum for DM features. We found that the DM took ~7 ms to excite with error bars from analyzing statistics of the experiment. We employed the identical procedure for the BUM, restricting our inspection to long pulse heating cycles when it became evident that the BUM was not excited by the short pulses. We found that the BUM took ~200 ms to excite. To measure the relaxation times, we examined the transition between long and short pulse heating. Again, slicing the spectrograms along constant time, we examined the frequency spectrum during a short pulse heating for persistent features of the DM/BUM that were previously excited during long pulsed heating. We found no evidence of persistent features, indicating that the DM and BUM both relax in under 1 s. Our excitation and relaxation times are consistent with the results presented by *Sergeev et al.* [2013] who found that the excitation time for the DM is under 20 ms, while that for the BUM is much longer. After noting the hysteresis effect discussed above, we also sought to observe the characteristic hysteresis time scale. To compute this, for the DM and the BUM separately, we tracked the time taken to return to the frequency corresponding to the maximum SEE

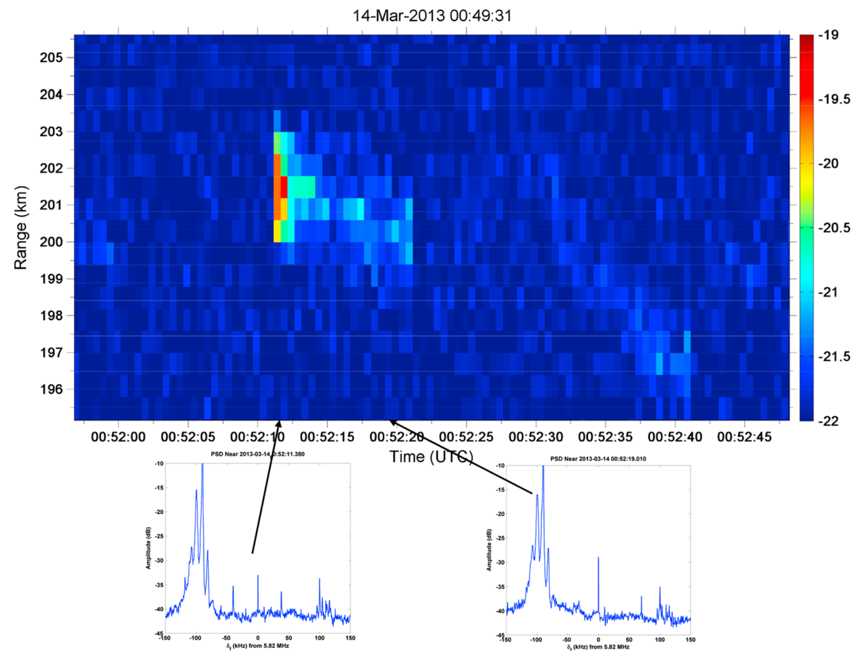

Figure 7. MUIR measurements taken at HAARP 14 March 2013 at 00:52:00– > 00:52:45 with selected SEE PSDs. Width of heated region is ~3–4 km; SEE spectrum indicates the presence of only DM during this measurement.

amplitude on the forward sweep to the maximum amplitude of the backward sweep. We found the BUM's hysteresis return time was ~200 s, while the DM's was ~300 s.

4. Discussion

It can be shown (see Appendix A) that $\delta n/n$, the relative change in electron density in the heated region, is directly proportional to the fluctuation in the STEC measurements, and inversely proportional to the width of the turbulent layer formed by the HF heating. We find that our ionograms from experiment #4 (see Figure 6) combined with the known GPS frequencies indicate the width of the heated region to be ~3–4 km, and this is consistent with MUIR's measurements (see Figure 7). Combining the size of the turbulent region with STEC fluctuations mentioned above, we found that during the HF heating that excited a DM in the SEE, $\delta n/n = 5$–7%, while during heating which excited a BUM, $\delta n/n = 20$–30%. The strong scattering of the GPS in the presence of the BUM in the SEE spectrum, indicates that SSS are connected to electron Bernstein modes, as predicted by *Gurevich and Zybin* [2006]. Note that in this experiment, $\delta n/n$ was measured indirectly through differential phase measurements of the GPS signal from PRN 07. It may be useful in the future to confirm these results, such as through direct measurements of the amplitude of the scattered signal.

4.1. Striation Relaxation Time Scale

A likely mechanism for the relaxation of striations is ambipolar diffusion. For a long cylindrical plasma column, the coefficient of ambipolar diffusion can be approximated by the electron diffusion across the geomagnetic field [*Chen*, 1977]

$$D_a = \frac{T_e \nu_{ei}}{m\,\omega_{ec}^2} = \frac{v_{th}^2}{2}\frac{\nu_{ei}}{\omega_{ec}^2}$$

where $\mathbf{v_{th}}$ is the electron thermal velocity and $\boldsymbol{\nu}_{\mathbf{ei}}$ is the electron-ion collision frequency.

$$\nu_{ei}\left(s^{-1}\right) = 2.9\times10^{-6} n_e \ln\Lambda / T_e^{3/2}$$

Here the coulomb logarithm is $\ln\Lambda = 23 - \ln\left(n_e^{1/2} T_e^{3/2}\right)$, the electron temperature is in eV, and the electron density is in cm^{-3}. For the ambient $T_e = 0.15$ eV, and $n_e = 4.5 \times 10^5$ cm^{-3} which corresponds to the plasma density that reflects 6 MHz heating radio wave, we obtain $\nu_{ei} = 300$ s^{-1} and $D_a = 0.1$ m^2/s, respectively.

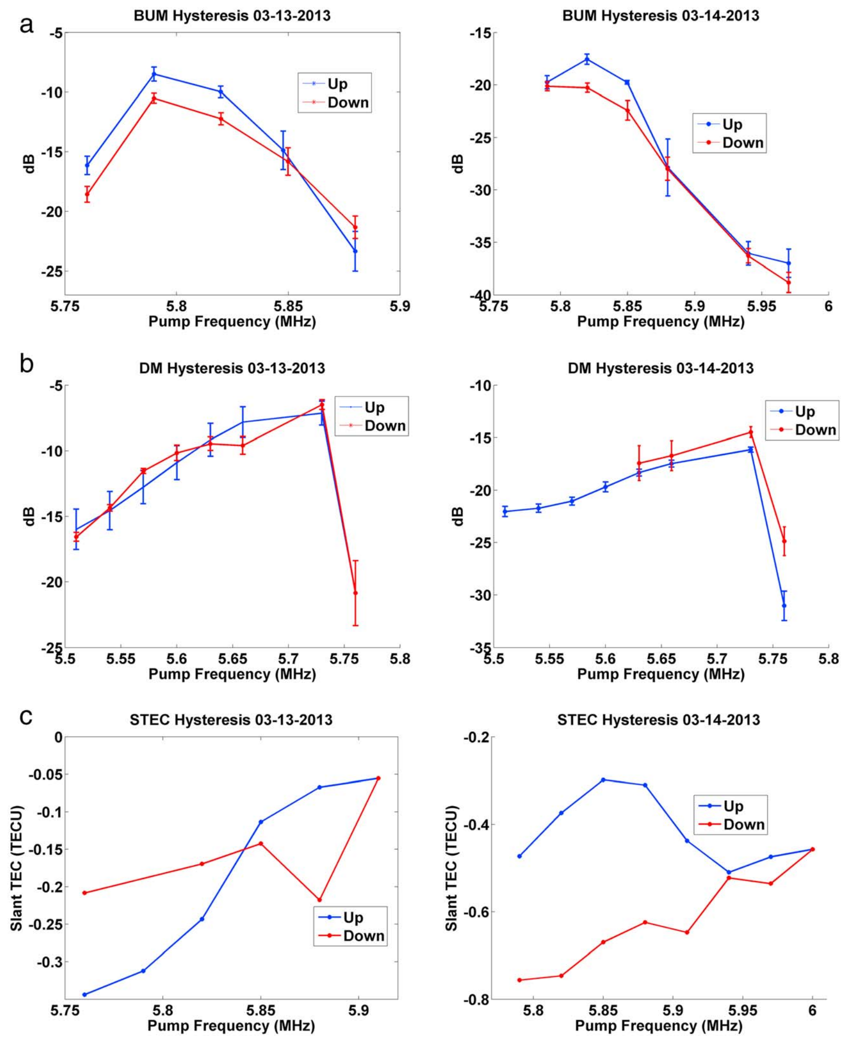

Figure 8. Hysteresis of (a) BUM, (b) DM, and (c) STEC measured on 13 March and 14 March. In all plots, forward or "up" sweep is indicated in blue, backward or "down" sweep is indicated in red.

Furthermore, the characteristic time scale of the SSS relaxation $\tau^{(1)} = \left(a_{\perp}^{\mathrm{sss}}\right)^2/D_a \simeq 0.4$ s since the typical spatial scale of Bernstein waves is $a_{\perp}^{\mathrm{sss}} = 0.2$ m. The value $\tau^{(1)}$ is consistent with the relaxation time of BUM that is less than 1 s detected from our experiments (see Table 2).

The experimental observations verify that striations of various length scales are being excited; there remains a question as to why their features, either from the SEE or STEC observations, exhibit hysteresis under a frequency sweep. The persistence of striations through cycles of HF heating could provide a mechanism for hysteresis.

We consider next the hysteresis related to the DM. According to Figure 8b, the PSD of up sweep frequency has lower amplitude than that of down sweep frequency, obtained at later times. A possible explanation can be that "the system memory" is long enough; thus, when revisiting the same heating frequency, some striations still exist and combined with the newly born striations magnify the SEE. *Norin et al.* [2008] estimated the transverse length of the striations involved in generation of the DM, as 7–30 m. Their relaxation time is $\tau^{(2)} = \left(a_{\perp}^{\mathrm{DM}}\right)^2/D_a > 500$ s. Thus, the ambipolar

Table 2. Summary of Time Scales Obtained From Our Experiment

Time Scale	BUM	DM
Excitation	200 ± 80 ms	6.5 ± 1.3 ms
Relaxation	<1 s	<1 s
Hysteresis	~200 s	~300 s

diffusion in our experiment cannot wash out the striations in 300 s (see Table 2), which could cause the DM-related hysteresis.

We consider next the hysteresis related to the BUM. According to Figure 8b, the PSD of up sweep frequency has higher amplitude than that of down sweep frequency, obtained at later times. This requires different mechanism than above for the DM hysteresis. We suggest that the BUM-related hysteresis is due to the large-scale striations that are scattering the pumping HF waves. The system memory is long enough; thus, those striations will survive during the time between two consecutive frequency sweeps.

We proceed with some estimates based on the scattering model of a rough surface [*Gurevich et al.*, 1997]. The model found scattering index f_{dif} that shows how much of the scattered energy is emitted in a particular direction within the solid angle

$$P/P_0 = \int f_{\mathrm{dif}} \mathrm{d}\Omega \simeq \frac{16\pi^2 a_\perp^2}{\lambda^2}\left(\frac{\Delta n_e}{n_e}\right)^2$$

Figure 8a shows that the BUM hysteresis produces 2–3 dB of the amplitude reduction on the difference between the up and down frequency sweeps. Assuming linear dependence of the SEE amplitude from the amplitude of the pumping wave, we find that

$$\frac{a_\perp}{\lambda}\frac{\Delta n_e}{n_e} \simeq 0.5 - 0.6$$

In fact, consider that an average density perturbation due to HF heating is about a few percent and that the wavelength of the pump wave is 50 m, we find that the most scattering effect is due to the long-scale striations having λ of the order of 1 km. Moreover, the ambipolar diffusion time for these kilometer-scale striations is ~1500 s, which is much longer than our hysteresis time scale for the BUM.

The key correlation that we noted in these experiments relates these various features

1. DM correlates with a weak to moderate STEC fluctuations (Figure 5) and with compact *F* layer (Figure 6a).
2. BUM correlates with a strong STEC fluctuations (Figure 5) and with spread *F* layer (Figure 6b).

In the first case, the DM indicates that no SSS are formed, while in the second case, the BUM indicates the formation of SSS through the four wave process followed by generation of strong turbulence. It is expected that the strong turbulence leads to the electron acceleration that ionizes the neutral atmosphere and thus forms the spread *F*.

This is similar to the phenomenon known as descending artificial ionized layer (DAIL) [*Pedersen et al.,* 2010] that begins with the strong Langmuir turbulence; pumped by HF heating, the turbulence accelerates electrons that in turn form new ionized layers below the original [*Eliasson et al.*, 2012]. In this multistep process, the DAIL starting from 200 to 210 km descends to 150 to 130 km height. In fact, ionograms made during the DAIL appearance show spread *F* gradually descending to the low altitudes [*Pedersen et al.*, 2010]. However, DAIL is formed only when the HF beam is directed along the magnetic zenith and the beam intersects the newly ionized layer, perturbing it, and producing additional hot electrons. In our observations, the beam was 20° off magnetic zenith (MZ); thus, we see the initial ionization, or starter of the DAIL, but the ionized region cannot propagate downward as it is not intersected by the HF beam.

In conclusion, two different diagnostic techniques, one measuring the differential phase of GPS signals, while another measuring the SEE response, were used simultaneously to study small-scale striations generated by the HAARP heater. These diagnostics were complemented by ionograms and incoherent radar data.

It was found that

1. In all cases that were examined, STEC begins fluctuating at the period of heating cycles (~20 s) within ~30–35 s after heating commences.
2. STEC measurements indicate that density perturbations vary from ~5% below gyroresonance, to 20–30% above, when BUM appears. Such striations can also affect UHF signals including GPS communications, and thus can be important in other applications.
3. Ionograms indicate that the presence of a BUM in the SEE spectrum is associated with strong ionospheric turbulence.

4. Of the six experiments performed, three have been examined in close detail, and all three indicated the presence of strong turbulence, similar to that observed in DAIL experiments [*Pedersen et al.*, 2010]. This turbulence is capable of accelerating bulk electrons, and in one of the experiments, the presence of these fast electrons was confirmed by MUIR.
5. Hysteresis was detected and is different for the BUM and the DM frequency ranges, indicating that the hysteresis may have two distinct mechanisms. We propose that the DM hysteresis is caused by persistent medium-scale striations (7–30 m) which combine with the newly excited striations to amplify the SEE. By contrast, the BUM hysteresis is due to persistent larger scale (km) striations which scatter the pump wave, reducing the efficiency of further heating.

Appendix A

The phase change of a GPS signal of frequency ω passing through the perturbed region of the ionosphere is given by *Milikh et al.* [2008]

$$\Delta\varphi = \frac{\omega}{c}\int \varepsilon dz \approx \frac{\omega}{c}\frac{\omega_e^2}{\omega^2}\frac{\delta n_e}{n_e} l \tag{A1}$$

where $\boldsymbol{\varepsilon}$ is the refraction index, $\omega_e = \sqrt{\mathbf{4\pi e^2 n_e/m}}$ is the electron plasma frequency, δn is the electron density perturbations due to the HF heating, and l is the length of the ray inside the perturbed region. From the above, the differential carrier phase $\boldsymbol{\Delta\phi_{12}}$ of two rays with frequencies f_1 and f_2 crossing the perturbed region is given by

$$\Delta\varphi_{12} = \frac{2\pi f_2}{c}\frac{f_{ep}^2}{f_2^2}\left(1 - \frac{f_2}{f_1}\right)\frac{\delta n_e}{n_e} l \tag{A2}$$

Applying this to the results of experiment #4 on 14 March 2013 for the frequencies of the L1 and L2 satellites and for heating frequency and thus f_{ep} close to 5.8 MHz, we obtain that

$$\Delta\varphi_{12}(\text{rad}) \simeq 0.13\frac{\delta n_e}{n_e} l(\text{km}) \tag{A3}$$

Finally by taking into account the relation 1 between the STEC and differential carrier path, we estimate relative perturbations of the electron density leading to GPS scattering

$$\frac{\delta n_e}{n_e} \simeq 4.37\frac{\Delta(\text{STEC})}{l(\text{km})} \tag{A4}$$

The artificial turbulence is confined in a layer between the HF wave reflection height z_0 and the upper hybrid height z_{uh} $\left(\mathbf{f_{ep}(z_0) = f_0; f_{ep}(z_{uh}) = \sqrt{f_0^2 - f_{ec}^2}}\right)$. Using the ionogram obtained during experiment #4 when $\mathbf{f_0}$ = 5.66 MHz while $\mathbf{f_{ep}(z_{uh})}$ = 5.49 MHz, we find that $\mathbf{l = z_0 - z_{uh} \simeq 3 - 4\ km}$.

Acknowledgments
All raw data for this paper are available for download via FTP at http://ftp.astro.umd.edu/pub/SPP/GRL_SSS_paper_data/, and Amir C. Najmi (anajmi1@umd.edu) may be contacted directly for access to either the whole data set or subsets of interest. This work was supported by DARPA via a subcontract N684228 with BAE Systems and also by the MURI grants N000140710789 and FA95501410019. The work at the Naval Research Laboratory was supported by the NRL 6.1 Base Program. We acknowledge very useful discussions with Alex Gurevich, Mike McCarrick's expert help in conducting the HAARP experiment, and Brenton Watkins' valuable contribution of the MUIR data.

Michael Balikhin thanks Robert Moore and an anonymous reviewer for their assistance in evaluating this paper.

References

Bakhmet'eva, N. V., V. N. Bubukina, Y. I. Ignat'ev, G. S. Bochkarev, V. A. Eremenko, V. V. Kol'tsov, I. V. Krasheninnikov, and Y. N. Cherkashin (1997), Investigation by backscatter radar of artificial irregularities produced in ionospheric plasma heating experiments, *J. Atmos. Sol. Terr. Phys.*, *59*, 2257–2263.
Bernhardt, P. A., C. A. Selcher, R. H. Lehmberg, S. Rodriguez, J. Thomason, M. McCarrick, and G. Frazer (2009), Determination of the electron temperature in the modified ionosphere over HAARP using the HF pumped Stimulated Brillouin Scatter (SBS) emission lines, *Ann. Geophys.*, *27*, 4409–4427.
Bernhardt, P. A., C. A. Selcher, and S. Kowtha (2011), Electron and ion Bernstein waves excited in the ionosphere by high power EM waves at the second harmonic of the electron cyclotron frequency, *Geophys. Res. Lett.*, *38*, L19107, doi:10.1029/2011GL049390.
Carozzi, T. D., B. Thide, S. M. Grach, T. B. Leyser, M. Holz, G. P. Komrakov, V. L. Frolov, and E. N. Sergeev (2002), Stimulated electromagnetic emissions during pump frequency sweep through fourth electron cyclotron harmonic, *J. Geophys. Res.*, *107*(A9), 1253, doi:10.1029/2001JA005082.
Carpenter, G. B. (1974), VHF and UHF bistatic observations of a region of the ionosphere modified by a high power radio transmitter, *Radio Sci.*, *9*, 965–969, doi:10.1029/RS009i011p00965.
Chen, F. F. (1977), *Introduction to Plasma Physics*, Premium Press, New York.
Dhillon, R., and T. R. Robinson (2005), Observations of time dependence and aspect sensitivity of regions of enhanced UHF backscatter associated with RF heating, *Ann. Geophys.*, *23*, 75–85.

Eliasson, B., X. Shao, G. Milikh, E. V. Mishin, K. Papadopoulos (2012), Numerical modeling of artificial ionospheric layers driven by high-power HF-heating, *J. Geophys. Res.*, *117*, A10321, doi:10.1029/2012JA018105.

Fialer, P. A. (1974), Field-aligned scattering from a heated region of the ionosphere—Observations at HF and VHF, *Radio Sci.*, *9*, 923–940, doi:10.1029/RS009i011p00923.

Gurevich, A. V. (2007), Nonlinear effects in the ionosphere, *Physics-Uspekhi*, *50*, 1091–1121, doi:10.1070/PU2007v050n11ABEH006212.

Gurevich, A. V., and K. P. Zybin (2006), Strong field aligned scattering of UHF radio waves in ionospheric modification, *Phys. Lett. A*, *358*, 159–165.

Gurevich, A. V., N. D. Borisov, and G. M. Milikh (1997), *Physics of Microwave Discharge: Artificial Ionized Regions in the Atmosphere*, Gordon and Breach, Amsterdam, Netherlands.

Hansen, J. D., G. J. Morales, L. M. Duncan, and G. Dimonte (1992), Large scale HF-induced ionospheric modifications experiments, *J. Geophys. Res.*, *97*, 113, doi:10.1029/91JA02403.

Kelley, M. C., T. L. Arce, J. Salowey, M. Sulzer, W. T. Armstrong, M. Carter, and L. Duncan (1995), Density depletions at the 10-m scale induced by the Arecibo heater, *J. Geophys. Res.*, *100*, 17,367, doi:10.1029/95JA00063.

Milikh, G. M., A. V. Gurevich, K. P. Zybin, and J. Secan (2008), Perturbations of GPS signals by the ionospheric irregularities generated due to HF-heating at triple of electron gyrofrequency, *Geophys. Res. Lett*, *35*, L22102, doi:10.1029/2008GL035527.

Norin, L., S. M. Grach, T. B. Leyser, B. Thide, E. N. Sergeev, and M. Berlin (2008), Ionospheric plasma density irregularities measured by stimulated electromagnetic emission, *J. Geophys. Res.*, *113*, A09314, doi:10.1029/2008JA013338.

Pedersen T., B. Gustavsson, and E. Mishin (2010), Creation of artificial ionospheric layers using high-power HF waves, *Geophys. Res. Lett.*, *37*, L02106, doi:10.1029/2009GL041895

Pelgrum W., Y. Morton, F. Graas, and S. Gunawardena (2011), Measurement and analysis of artificially-generated and natural ionosphere scintillations effects on GNSS signals, Proc. ION ITM, 950-958,

Rao, P. B., and G. D. Thome (1974), A model for RF scattering from field-aligned heater-induced irregularities, *Radio Sci.*, *9*, 987–996, doi:10.1029/RS009i011p00987.

Sergeev, E., S. Grach, A. Shindin, E. Mishin, P. Bernhardt, S. Briczinski, B. Isham, M. Broughton, J. LaBelle, and B. Watkins (2013), Artificial ionospheric layers during pump frequency stepping near the 4th gyroharmonic at HAARP, *Phys. Rev. Lett.*, *110*, doi:10.1103/PhysRevLett.110065002.

Thide, B., H. Kopka, and P. Stubbe (1982), Observations of stimulated scattering of a strong high-frequency radio wave in the ionosphere, *Phys. Rev. Lett.*, *49*, doi:10.1103/PhysRevLett.49.1561.

Thome, G. D., and D. W. Blood (1974), First observations of RF backscatter from field-aligned irregularities produced by ionospheric heating, *Radio Sci.*, *9*, 917–921, doi:10.1029/RS009i011p00917.